Observability coefficients for predicting the class of synchronizability from the algebraic structure of the local oscillators

Irene Sendiña-Nadal,[1,2] Stefano Boccaletti,[3,4] and Christophe Letellier[5]
[1]*Complex Systems Group, Universidad Rey Juan Carlos, E-28933 Móstoles, Madrid, Spain*
[2]*Center for Biomedical Technology, Universidad Politécnica de Madrid, E-28223 Pozuelo de Alarcón, Madrid, Spain*
[3]*CNR-Institute of Complex Systems, Via Madonna del Piano, 10, I-50019 Sesto Fiorentino, Florence, Italy*
[4]*Italian Embassy in Israel, 25 Hamered Street, 68125 Tel Aviv, Israel*
[5]*CORIA UMR 6614—Normandie Université, CNRS et INSA de Rouen, Campus Universitaire du Madrillet, F-76800 Saint-Etienne du Rouvray, France*
(Received 23 May 2016; published 7 October 2016)

Understanding the conditions under which a collective dynamics emerges in a complex network is still an open problem. A useful approach is the master stability function—and its related classes of synchronization—which offers a necessary condition to assess when a network successfully synchronizes. Observability coefficients, on the other hand, quantify how well the original state space of a system can be *observed* given only the access to a *measured* variable. The question is therefore pertinent: Given a generic dynamical system (represented by a state variable $\boldsymbol{x}$) and given a generic measure on it $h(\boldsymbol{x})$ (which may be either an observation of an external agent, or an output function through which the units of a network interact), are classes of synchronization and observability actually related to each other? We explicitly address this issue, and show a series of nontrivial relationships for networks of different popular chaotic systems (Rössler, Lorenz, and Hindmarsh-Rose oscillators). Our results suggest that specific dynamical properties can be evoked for explaining the classes of synchronizability.

DOI: 10.1103/PhysRevE.94.042205

I. INTRODUCTION

The word *synchronization*, from the Greek $\sigma\upsilon\nu$ (together) and $\chi\rho\sigma\nu\sigma$ (time), means "happening at the same time," and appeared in 1620 at a time where determining longitudes was a major problem for transoceanic voyages. In order to solve it, Christian Huygens invented the pendulum clock (1657) and investigated two simultaneously operating maritime clocks (as two clocks were required for practical purposes in the case one clock was stopped). He thus found that clocks were synchronized [1] when they were close and oscillating in the same plane: In fact, they were antiphase synchronized. Since that time, synchronization was investigated in various fields as in mechanics [2], chemistry [3], neuroscience [4,5], biology [6], ecology [7], social interactions [8], and is now a topic sufficiently mature for deserving dedicated works [9–11]. In particular, synchronization has been used as a tool for estimating model parameters in global modeling from experimental data [12–14] and also for network structure detection using Bayesian dynamical inference [15,16] and mutual information methods [17].

One of the most relevant problems in synchronization is the *a priori* determination of which conditions allow oscillators to synchronize or not. One of the most elegant solutions is provided by the so-called master stability function (MSF) introduced by Pecora and Carroll [18], which gives a necessary (but not sufficient) condition under which a specific coupling (network) configuration leads to a synchronous evolution for a particular (local) oscillator dynamics. Later on, it was shown that, close to a threshold, all possible choices of local dynamics and output functions reduce actually to only three classes of synchronization, each one identified with a specific behavior of the MSF [19]. These theoretical concepts are very efficient for identical oscillators, and remain valid for nearly identical systems.

On the other hand, it is known that the coupling function strongly affects the system's synchronizability [20,21] and the quality of the exchanged information depends on the variables used to transmit the oscillators' state. Issued from the control theory, the concept of observability was introduced to address such a quality [22], and later on, observability coefficients were defined to quantify it with a real number [23,24]. Observability coefficients account for how faithfully the state space of a dynamical system can be reconstructed from a time series of some of its measured variables. Observability is now a concept considered as relevant for investigating networks since, for large dimensional systems, being able to accurately observe the whole dynamics just from a limited set of variables is fundamental [25,26]. This is particularly relevant for plant instrumentation [27], network control [28], power grid stability [29], or global modeling [30].

The easiness with which a given system can be synchronized to one or few of its copies is still difficult to assess from its algebraic structure, and constructing a synchronizability index for a quantitative comparison of different systems remains an open problem [31–34]. Recently, it was shown that the observability coefficients could contribute to such an index [35,36], suggesting that the quality of the information about the state of each system transmitted to the others is indeed an ingredient to consider for explaining synchronizability. Nevertheless, observability does not fully explain the synchronization phenomenon and, a dynamical component—more related to the parameter values than to the algebraic structure of the governing equations—is, sometimes, evoked for explaining it [31,35].

In the present work, we will investigate whether the types of MSFs—or the so-called classes of synchronization—are related to observability using three popular chaotic systems in network theory, namely the Rössler system, the Lorenz system,

and the Hindmarsh-Rose system. Since a dynamical component could contribute to the synchronization phenomenon, we will investigate how synchronizability (and observability) could depend on parameter values. Section II is devoted to the theoretical background used throughout this work, that is, to the observability coefficients and the classes of synchronization. Section III, which is the main part of this paper, discusses the cases of the three considered systems. Section IV gives some conclusions.

II. THEORETICAL BACKGROUND

A. Observability

Let

$$\dot{\boldsymbol{x}} = \boldsymbol{f}(\boldsymbol{x}) \tag{1}$$

be a dynamical system where $\boldsymbol{x} \in \mathbb{R}^m$ is its corresponding m-dimensional state space. Let $h : \boldsymbol{x} \mapsto s$ be the measurement function where s is the (scalar) variable used to observe the state space. A space can be reconstructed from these measurements $\{s(t)\}$ by using derivatives or delay coordinates [37]. When derivative coordinates are used, the function $\Phi : \mathcal{A}_{\mathrm{O}} \in \mathbb{R}^m \mapsto \mathcal{A}_{\mathrm{R}} \in \mathbb{R}^m$ allows one to assess the observability of the attractor $\mathcal{A}_{\mathrm{O}}$ from the original space using the measured variable s [24]. This can be performed with the help of the control theory by constructing the so-called *observability matrix* which is rigorously defined as [38]

$$\mathcal{O} = \begin{bmatrix} dh(\boldsymbol{x}) \\ d\mathcal{L}_f h(\boldsymbol{x}) \\ \cdots \\ d\mathcal{L}_f^j h(\boldsymbol{x}) \end{bmatrix}, \tag{2}$$

where $\mathcal{L}^k$ is the kth order Lie derivative, with $j \geqslant m-1$ [39].

The observability matrix $\mathcal{O}$ corresponds in fact to the Jacobian matrix of the map Φ between the original attractor $\mathcal{A}_{\mathrm{O}}$ and the reconstructed one $\mathcal{A}_{\mathrm{R}}$ when derivative coordinates are used [24]. Rather than using the full rank theorem to assess the observability—thus providing a yes-or-no answer—we prefer to use here the observability coefficients η_{s^m} which are real numbers in the unit interval, 0 referring to a full lack of observability and 1 to a full observability [23]. When $\eta_{s^m} = 1$, the map Φ is a diffeomorphism. It was shown that the decrease of the observability coefficient is strongly related to the order of the determinant of the observability matrix Det $\mathcal{O}$ (= Det $\mathcal{J}_{\Phi_s}$) [23]. Considering that an order-1 determinant Det $\mathcal{O}$ provides a good observability compared to a second-order determinant, we computed a receiver operating characteristic (ROC) to determine the threshold on the symbolic observability coefficients above (below) which the observability can be considered as good (poor) using the observability coefficients reported in Ref. [40]. The ROC curve (Fig. 1) suggests a threshold between 0.74 and 0.75. We retained $\eta_{\mathrm{c}} = 0.75$ as the threshold value above which the observability is considered as good. For a symbolic computation of these coefficients from the symbolic Jacobian matrix of system $\boldsymbol{f}$, the reader may refer to Refs. [40,41]. It was shown that these observability coefficients may partly explain the quality of synchronizability observed between two systems, but there are other components contributing to synchronizability which remains to be understood [35,36].

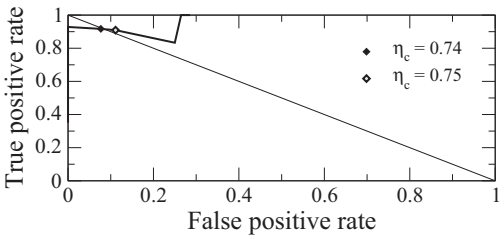

FIG. 1. ROC curve for distinguishing between good and poor observabilities.

As commonly considered in the control theory, observability does not depend on the underlying dynamics since it is not related to parameter values; indeed it only depends on the algebraic structure of the vector field. By definition, the symbolic observability coefficients (as introduced in Refs. [40,41]) are not dependent on parameter values. Nevertheless, it was shown that the observability coefficients can be numerically assessed by considering the probability for visiting the neighborhood of the singular observability manifold defined as [42]

$$\mathcal{U}_{\mathcal{M}_s^{\mathrm{obs}}} = \{(x,y,z) \in \mathbb{R}^3 || \mathrm{Det}\ \mathcal{J}_{\Phi_s}| < \delta\}, \tag{3}$$

where

$$\delta = \mu\big[\mathrm{Max}\left(\mathrm{Det}\ \mathcal{J}_{\Phi_s}\right) - \mathrm{Min}\left(\mathrm{Det}\ \mathcal{J}_{\Phi_s}\right)\big], \tag{4}$$

with $\mu = 0.05$. This latter value is quite arbitrary but we checked that the results are robust when it is slightly modified. A coefficient taking into account the way the singular observability manifold $\mathcal{M}_s^{\mathrm{obs}}$ is visited is thus defined according to

$$\eta_s^{\mathrm{man}} = \left(1 - \overline{T}_{\mathcal{M}_s^{\mathrm{obs}}}\right)\left(1 - P_{\mathcal{M}_s^{\mathrm{obs}}}\right), \tag{5}$$

where $T_{\mathcal{M}_s^{\mathrm{obs}}}$ is the relative time with which the trajectory remains during a time $\tilde{T}_{\mathcal{M}_s^{\mathrm{obs}}}$ in the neighborhood $\mathcal{U}_{\mathcal{M}_s^{\mathrm{obs}}}$ divided by the pseudoperiod T_0 of the system (the mean time interval between two consecutive intersections with a Poincaré section). $P_{\mathcal{M}_s^{\mathrm{obs}}}$ is the probability for a trajectory $\{\boldsymbol{x}_n\}_{n=0}^N$ of measured points to be in the neighborhood $\mathcal{U}_{\mathcal{M}_s^{\mathrm{obs}}}$ of the singular observability manifold $\mathcal{M}_s^{\mathrm{obs}}$, that is, the probability for a point of the attractor $\mathcal{A}_{\mathrm{O}}$ to be associated with

$$\left|\mathrm{Det}\mathcal{J}_{\Phi_s}\right| < \delta. \tag{6}$$

When the probability to have points $\boldsymbol{x} \in \mathcal{A}_{\mathrm{O}} \bigcap \mathcal{M}_s^{\mathrm{obs}}$ increases, the number of points for which the original dynamics is not observable increases. Coefficients η_s^{man} are designed as the manifold observability coefficients. By definition, these coefficients depend on the way the solution of the system considered visits the state space and, consequently, how it visits the neighborhood of the singular observability manifold: One may thus expect that the manifold observability coefficients depend on parameter values.

B. Master stability function

Let us consider a network of N identical oscillators (1) governed by [18]

$$\dot{\boldsymbol{x}}_i = \boldsymbol{f}(\boldsymbol{x}_i) - \epsilon \sum_{j=1}^{N} G_{ij} \boldsymbol{h}(\boldsymbol{x}_j), \tag{7}$$

where $\boldsymbol{h}(\boldsymbol{x}_j)$ is a measurement function according to which all oscillators are observed, and G_{ij} is a coupling matrix satisfying $\sum_{j=1}^{N} G_{ij} = 0$ for any $i \in [1; N]$. ϵ is a global coupling parameter. By definition, the synchronization manifold is such as $\boldsymbol{x}_i = \boldsymbol{x}^{\mathrm{s}}$ $(\forall i \in [1; N])$ and verifies $\dot{\boldsymbol{x}}^{\mathrm{s}} = \boldsymbol{f}(\boldsymbol{x}^{\mathrm{s}})$. The variational equation associated with the governing Eq. (7) of our network is

$$\dot{\boldsymbol{\xi}}_i = \mathcal{J}_{\boldsymbol{f}}(\boldsymbol{x}^{\mathrm{s}})\boldsymbol{\xi}_i - \epsilon \sum_{j=1}^{N} G_{ij} \mathcal{J}_{\boldsymbol{h}}(\boldsymbol{x}^{\mathrm{s}})\boldsymbol{\xi}_j, \tag{8}$$

where $\boldsymbol{\xi}_i = \boldsymbol{x}_i - \boldsymbol{x}^{\mathrm{s}}$ designates the evolution of the perturbed synchronous solution, and where $\mathcal{J}_{\boldsymbol{f}}(\boldsymbol{x}^{\mathrm{s}})$ and $\mathcal{J}_{\boldsymbol{h}}(\boldsymbol{x}^{\mathrm{s}})$ are the $m \times m$ Jacobian matrices of the vector field $\boldsymbol{f}$ and the measurement function $\boldsymbol{h}$, respectively. It is then assumed that the matrix $\boldsymbol{G}$ can be diagonalized, leading to the spectrum of eigenvalues $\boldsymbol{\nu} \in \mathbb{R}^N$. The variational equation can thus be rewritten as

$$\dot{\boldsymbol{\zeta}}_i = [\mathcal{J}_{\boldsymbol{f}}(\boldsymbol{x}^{\mathrm{s}}) - \epsilon \nu_i \mathcal{J}_{\boldsymbol{h}}(\boldsymbol{x}^{\mathrm{s}})]\boldsymbol{\zeta}_i, \tag{9}$$

where $\boldsymbol{\zeta}_i$ are the eigenvectors of matrix $\boldsymbol{G}$ verifying $0 = \nu_1 < \nu_2 \leqslant \cdots \leqslant \nu_N$. Setting $\mu_i = \epsilon \nu_i$, we thus obtain

$$\dot{\boldsymbol{\zeta}}_i = [\mathcal{J}_{\boldsymbol{f}}(\boldsymbol{x}^{\mathrm{s}}) - \mu_i \mathcal{J}_{\boldsymbol{h}}(\boldsymbol{x}^{\mathrm{s}})]\boldsymbol{\zeta}_i. \tag{10}$$

Let $\mu_i = \epsilon \nu_i$ $(i \in [2; N])$ be the coupling parameter values related to a normalized value μ, the variational equation can be decomposed into structurally equivalent blocks, only differing by the coupling parameter values μ_i. The generic variational equation for each block is thus

$$\dot{\boldsymbol{\zeta}} = [\mathcal{J}_{\boldsymbol{f}}(\boldsymbol{x}^{\mathrm{s}}) - \mu \mathcal{J}_{\boldsymbol{h}}(\boldsymbol{x}^{\mathrm{s}})]\boldsymbol{\zeta}. \tag{11}$$

The largest Lyapunov exponent Λ for this equation thus defines the MSF [18]. When it is negative, the synchronization manifold is stable and the whole set of N oscillators should evolve fully synchronized. Obviously, the Jacobian matrix $\mathcal{J}_{\boldsymbol{f}}$ depends on parameter values and so the MSF. One of our objectives is therefore to investigate how relevant is such a dependence in relation to the observability coefficients.

It was shown that there are three possible behaviors of the MSF in the vicinity of the origin depending on the choice of the $\boldsymbol{f}$ and $\boldsymbol{h}$ functions [19]. As it will be later justified, we here use a slightly modified terminology for the three possible classes of synchronizability, as follows.

(1) Class I corresponds to an MSF remaining negative for any $\mu > \mu_{\mathrm{m}}$, meaning that the networked systems can be synchronized for any coupling strength greater than a threshold value $\epsilon > \mu_{\mathrm{m}}/\nu_2$;

(2) Class II corresponds to an MSF being negative within a range $\mu \in [\mu_{\mathrm{m}}; \mu_{\mathrm{M}}]$, meaning that there is a finite interval for the coupling strength such that $\nu_N/\nu_2 < \mu_{\mathrm{M}}/\mu_{\mathrm{m}}$ where the networked systems can be synchronized;

(3) Class III corresponds to an MSF remaining positive for any μ value, meaning that the networked systems can never be synchronized for any coupling strength.

The three classes are thus numbered to be associated with the case providing the most synchronizable case (class I) to the worst synchronizable case (class III). Another set of classes, denoted as Γ_n, was proposed for the MSFs $\Lambda(\mu)$ by Huang and co-workers [43] according to the number n of zeros these functions have. There is therefore a direct correspondence between the previous three classes and Huang's classes. When the MSF has no zeros, it belongs to class Γ_0, that is, to class III since it is always positive. When there is a single zero (class Γ_1), the MSF remains negative for any $\mu > \mu_{\mathrm{m}}$; it thus corresponds to a class I synchronization. When the MSF has two zeros (class Γ_2), it is negative over a range $[\mu_{\mathrm{m}}; \mu_{\mathrm{M}}]$; this is thus a class II synchronization. Huang and co-workers also considered cases where $n > 2$, but we will not consider any of these cases in the present work as we focus on phenomena occurring close to the threshold for synchronization. Class II synchronization could be generalized as made of Γ_n $(n \geqslant 2)$. It is relevant to state that the values taken by the MSF $\Lambda(\mu)$ as well as the μ values at which $\Lambda(\mu) = 0$ are specific to the local oscillator as well as to the coupling measurement scheme: They cannot therefore be used to compare quantitatively the synchronizability presented by different systems as well as by a single system but coupled through different coupling schemes. Only the form, that is, the class of synchronization is meaningful. Our purpose is now to investigate, as it was suggested in Ref. [41], whether the synchronizability—or equivalently the class of synchronizability—is related to the observability coefficients.

III. RESULTS

A. Coupled Rössler systems

We investigate the Rössler system [44]:

$$\begin{aligned} \dot{x} &= -y - z, \\ \dot{y} &= x + ay, \\ \dot{z} &= b + z(x - c), \end{aligned} \tag{12}$$

for which parameter a is varied, $b = 2$, and $c = 4$, as investigated in Ref. [45]. Depending on the a value, the dynamics is phase coherent $(a \in [0.380; 0.43295])$, i.e., all revolutions around the central singular point are completed in a rather constant duration [46]. For a values greater than 0.43295, the attractor has a funnel structure characterized by secondary oscillations around an axis roughly connecting the two singular points [45]. Revolutions are thus completed in durations which strongly depend on the location of the trajectory within the attractor; the more peripheral the trajectory, the longer the revolution. Phase noncoherent dynamics in the Rössler system are always characterized by multimodal maps (the number of critical points—extrema—is greater than one) [45].

An analysis of the Rössler system by computing the symbolic observability coefficients $\eta_{s^3}^{\mathrm{sym}}$ leads to [40]

$$\eta_{y^3}^{\mathrm{sym}} = 1 \rhd \eta_{x^3}^{\mathrm{sym}} = 0.84 \rhd \eta_{z^3}^{\mathrm{sym}} = 0.56.$$

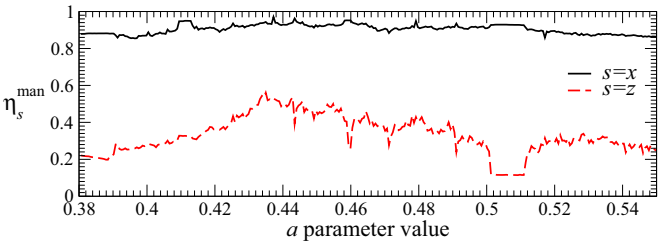

FIG. 2. Evolution of the manifold observability coefficients η_s^{man} for the Rössler system versus a parameter values.

As already mentioned, these coefficients do not depend on parameter values and express the fact that a full observability of the state space is obtained by measuring variable y (a property which does remain true for any parameter values), a rather good observability is obtained when variable x is measured, and a rather poor observability is found when variable z is measured. In order to assess whether the observability depends on parameter values, we computed the manifold observability coefficients $\eta_{x^3}^{\text{man}}$ and $\eta_{z^3}^{\text{man}}$ ($\eta_{y^3}^{\text{man}}$ being equal to 1 since the singular observability manifold $\mathcal{M}_y^{\text{obs}}$ is an empty set). The two other singular observability manifolds are

$$\mathcal{M}_x^{\text{obs}} = \{(x,y,z) \in \mathbb{R}^3 | x = a + c\}, \tag{13}$$

and

$$\mathcal{M}_z^{\text{obs}} = \{(x,y,z) \in \mathbb{R}^3 | z = 0\}. \tag{14}$$

The corresponding manifold observability coefficients $\eta_{x^3}^{\text{man}}$ and $\eta_{z^3}^{\text{man}}$ are plotted versus a values in Fig. 2. The mean values for the manifold observability coefficients are $\overline{\eta}_{x^3}^{\text{man}} = 0.90$ and $\overline{\eta}_{z^3}^{\text{man}} = 0.33$, two values which are in a rather good agreement with those provided by the symbolic observability coefficients. Even if the coefficient $\overline{\eta}_{z^3}^{\text{man}} = 0.33$ presents some variations versus a values (the standard deviation equals ± 0.10), its value remains significantly less than 0.75, meaning that the observability provided by variable z is poor.

This means that when two systems are coupled *via* variable y, one of the systems *has the full knowledge* of which phase space state is being visited by its companion, but it has far more rarely such information when instead variable z is measured. This is why the synchronizability, here defined as the ability of a given system to be synchronized with another one, strongly depends on the coupling variable [36,41].

Here we will consider coupling functions $\boldsymbol{h}(\boldsymbol{x})$ with one and two components in a situation where the ith component of one oscillator is coupled to the same component of another oscillator. When each variable is successively chosen as the coupling variable, the MSFs $\Lambda_s(\mu)$ are clearly of different types and do not depend on parameter values (Fig. 3). According to the definitions we introduced in Sec. II B, coupling Rössler systems *via* variable y [$\boldsymbol{h}(\boldsymbol{x}) = (0,y,0)$] leads to a class I synchronizability, that is, they can be synchronized for any value $\mu > \mu_{\text{m}}$ [see Fig. 3(b)]. When coupled *via* variable x [$\boldsymbol{h}(\boldsymbol{x}) = (x,0,0)$], Rössler systems present a class II synchronizability, thus meaning that they can be synchronized for a certain range $[\mu_{\text{m}};\mu_{\text{M}}]$ [Fig. 3(a)]. When variable z is used as the coupling variable [$\boldsymbol{h}(\boldsymbol{x}) = (0,0,z)$], only a class III synchronizability is obtained, meaning that it is impossible to synchronize two Rössler systems coupled by the variable z [Fig. 3(c)]. The conclusion is that, in the case of the Rössler system, the different classes of synchronizability associated with each variable are strongly related to the observability coefficients since a class I synchronizability is obtained with variable y providing a full observability, a class II synchronizability is obtained with variable x associated with an observability coefficient close to 1, and a class III synchronizability, that is, no synchronization, can be obtained when the systems are coupled *via* variables offering a very poor observability.

The coupling function $\boldsymbol{h}$ can also be chosen to map the state vector $\boldsymbol{x}$ into, for instance, a two-dimensional vector. When the latter occurs, i.e., a single variable s is used for coupling two systems, the single possibility to reconstruct the state space is to use the derivative coordinates as $(s,\dot{s},\ddot{s})$. The observability to relate with that variable is therefore nonambiguous. Contrary to this, when two variables are used to couple two systems, there are two possibilities to reconstruct the state space: $(s_1,s_2,\dot{s}_2)$ or $(s_1,\dot{s}_1,s_2)$. It is therefore no longer possible to determine in a nonambiguous way which observability has to be associated with a particular coupling scheme. For instance, when variables x and y [$\boldsymbol{h}(\boldsymbol{x}) = (x,y,0)$] are used to couple two Rössler systems, it is not clear how one system is seen by the other. Indeed, if the differentiable embedding is spanned by $(x,y,\dot{y})$, the symbolic observability $\eta_{xy^2} = 0$, meaning that the original state space is not observable at all! Now, if the differential embedding is spanned by $(x,\dot{x},y)$, the symbolic observability coefficient is $\eta_{x^2y} = 1$: the original state space is fully observable! The master stability function $\Lambda_{xy}(\mu)$ leads to a class I synchronization [Fig. 3(d)].

When Rössler systems are coupled using variables x and z [$\boldsymbol{h}(\boldsymbol{x}) = (x,0,z)$] is nearly similar from the observability point of view since $\eta_{xz^2} = 0$ and $\eta_{x^2z} = 1$. Nevertheless, the MSF Λ_{xz} leads to a class II synchronization. This result suggests that these two variables provide a mean observability $\overline{\eta}_{xz} = \eta_{x^3} + \eta_{z^3} = \frac{0.84+0.56}{2} = 0.70$ which is smaller than $\overline{\eta}_{xy} = \eta_{x^3} + \eta_{y^3} = \frac{0.84+1.00}{2} = 0.92$: This would confirm that the class of synchronization can be related, at least for the Rössler system, to the observability provided by the coupling variables. As observed in Ref. [47], coupling systems using two variables can improve the synchronizability: In our case, coupling two Rössler systems with variables x and y leads to a class I synchronization; compared to a coupling *via* variable x, the synchronization is improved (from class II to class I) since variable x is combined with a variable with a better observability. Contrary to this, when variable x is combined with variable z, the synchronizability is not improved and remains of class II as when Rössler systems were coupled by variable x.

Combining variables y and z [$\boldsymbol{h}(\boldsymbol{x}) = (0,y,z)$] for coupling Rössler systems could not improve the synchronizability from the observability point of view since a full observability is already obtained with the sole variable y. We already saw that combining variables y and x improves in fact the synchronizability, not by changing the class of synchronization but by increasing the negativity of the MSF [compare Figs. 3(d) and 3(b)]. When variable y is combined with variable z, a class I synchronization is obtained. Such a class of synchronization was observed with the sole variable y. In fact, the MSFs

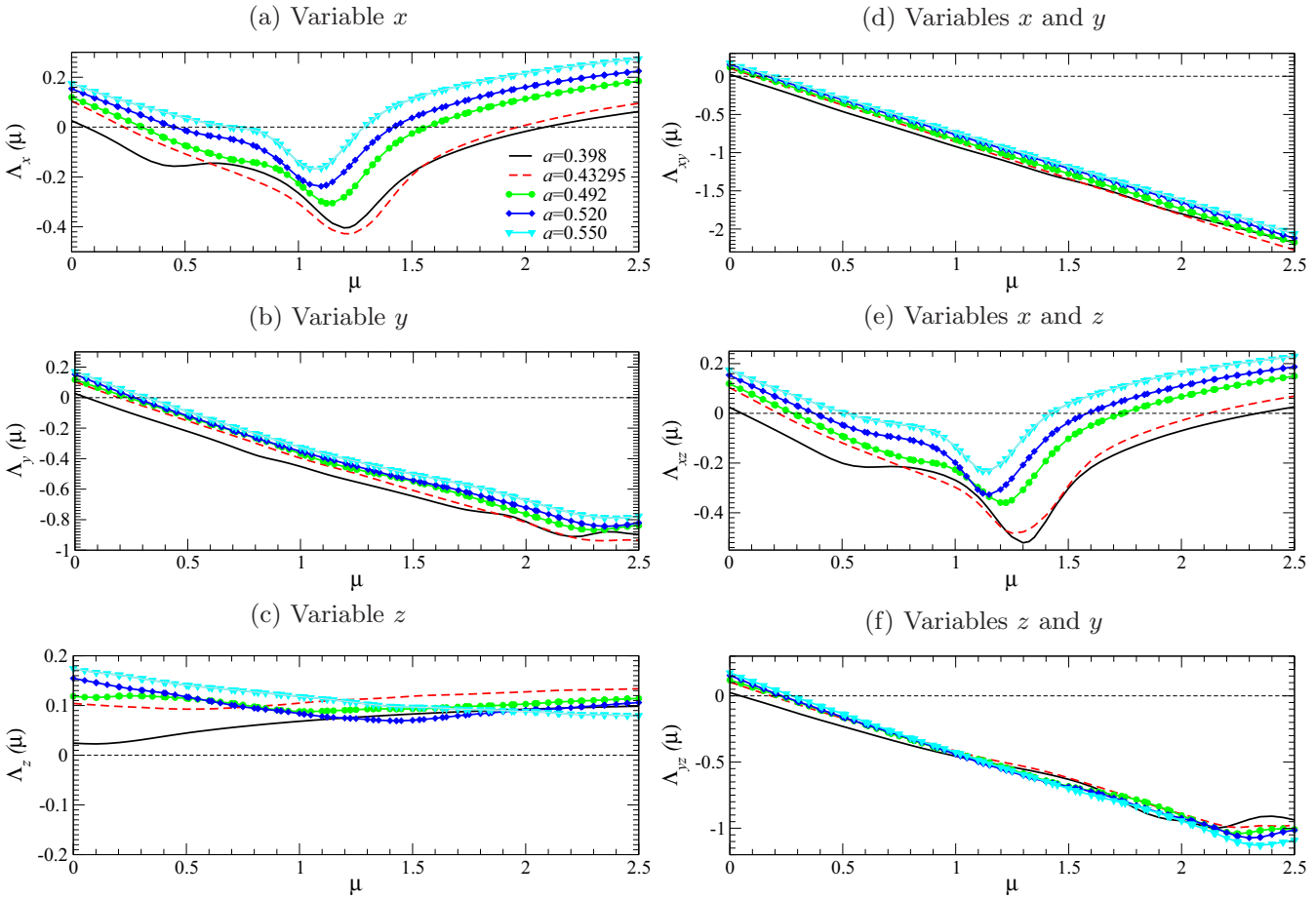

FIG. 3. Master stability functions $\Lambda_s(\mu)$ versus the normalized coupling parameter μ computed for Rössler systems coupled *via* each one of the three variables (a)–(c) and *via* a combination of two of its variables (d)–(f) and for different a values as shown in the legend of (a). Other parameter values are $b = 2$ and $c = 4$.

are almost not affected by adding variable z in the coupling scheme. Thus, depending on the variable first considered, it may be useful to combine a second variable for coupling the systems, or not. When variable y is used, the interest in adding a second variable is rather limited if variable x is chosen and, it has no significant effect on the synchronizability if variable z is added [compare Figs. 3(c) and 3(f)]. When variable x is first used for coupling Rössler systems, there is an interest in adding variable y since the synchronization switches from class II to class I but there is none in adding variable z.

In case the Rössler oscillators are coupled through the three variables, it is evident that the system is fully observable giving rise to a class I of synchronizability as is observed in Fig. 4.

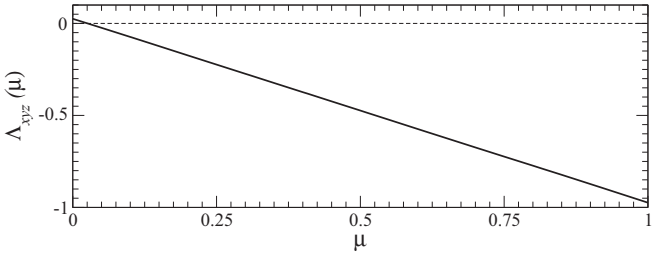

FIG. 4. Master stability function for Rössler systems coupled through the three variables with an output function $\boldsymbol{h}(\boldsymbol{x}) = (x, y, z)$.

B. Coupled Lorenz systems

We now consider the Lorenz system [48]:

$$\begin{aligned} \dot{x} &= \sigma(y - x), \\ \dot{y} &= Rx - y - xz, \\ \dot{z} &= -bz + xy, \end{aligned} \tag{15}$$

which is equivariant under an $\mathcal{R}_z$ rotation symmetry around the z axis [49,50]. Depending on parameter values, the Lorenz system can thus produce very different behaviors. In order to evaluate whether these different dynamics affect synchronizability or not, we considered two different lines in the parameter space. The first one is defined by $\sigma = 10$ and $b = \frac{8}{3}$ and two representative attractors are plotted in Fig. 5: the well-known "Lorenz attractor" for $R = 28$ [Fig. 5(a)] and the one with two coexisting asymmetric attractors for $R = 203.1$ [Fig. 5(b)]. The second one is defined by the line $\sigma = 30$ and $b = 1$ and is associated with the so-called "Burke and Shaw" attractor shown in Fig. 5(c) [51].

The symbolic observability coefficients for the Lorenz system are

$$\eta^{\text{sym}}_{x^3} = 0.78 > \eta^{\text{sym}}_{y^3} = 0.36 = \eta^{\text{sym}}_{z^3} = 0.36. \tag{16}$$

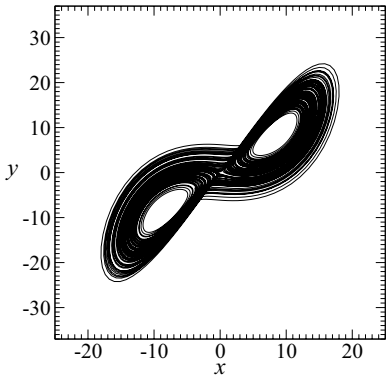

(a) $R = 28$, $\sigma = 10$, $b = \frac{8}{3}$

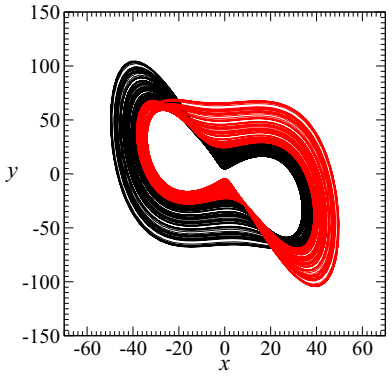

(b) $R = 203.1$, $\sigma = 10$, $b = \frac{8}{3}$

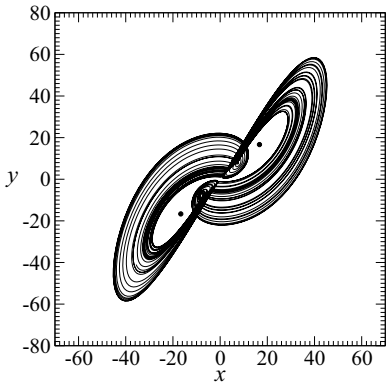

(c) $R = 278.8$, $\sigma = 30$, $b = 1$

FIG. 5. Three chaotic attractors produced by the Lorenz system for some parameter values. Two coexisting asymmetric attractors (one in black, one in red) are shown in (b).

These coefficients, by definition, only depend on the algebraic structure of the system. To investigate how observability may depend on parameter values, we also computed the manifold observability coefficients $\eta_{s^3}^{\text{man}}$ associated with the singular observability manifolds:

$$\mathcal{M}_x^{\text{obs}} = \{(x,y,z) \in \mathbb{R}^3 | \sigma^2 x = 0\}, \tag{17}$$

$$\mathcal{M}_y^{\text{obs}} = \left\{(x,y,z) \in \mathbb{R}^3 | z = R - \frac{Rbx}{\sigma y} + \frac{2x^2}{\sigma}\right\}, \tag{18}$$

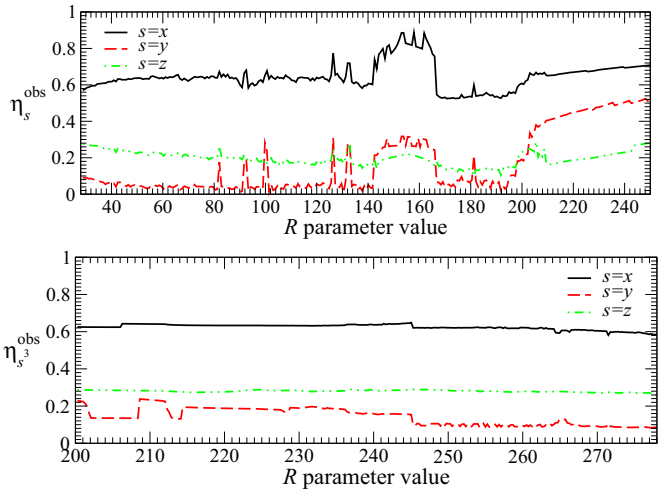

FIG. 6. Evolution of the manifold observability coefficients for the Lorenz system when $\sigma = 10$ and $b = \frac{8}{3}$ (top panel) and $\sigma = 30$ and $b = 1$ (bottom panel).

and

$$\mathcal{M}_z^{\text{obs}} = \left\{(x,y,z) \in \mathbb{R}^3 | z = R - \sigma\left(\frac{y}{x}\right)^2\right\}, \tag{19}$$

respectively. These coefficients are plotted versus R values in Fig. 6 for the two different types of attractors. The mean manifold observability coefficients are

$$\overline{\eta}_{x^3}^{\text{man}} = 0.65 > \overline{\eta}_{y^3}^{\text{man}} = 0.20 = \overline{\eta}_{z^3}^{\text{man}} = 0.20,$$

and, consequently, are in a good agreement with the symbolic observability coefficients: Variable x provides the best observability of the state space ($\eta_{x^3}^{\text{man}} > 0.60$). Variables y and z are associated with manifold observability coefficients which are clearly smaller than $\eta_{x^3}^{\text{man}}$. The manifold observability coefficients suggest that, for most of the R values (Fig. 6, $\eta_{z^3}^{\text{man}} > \eta_{y^3}^{\text{man}}$). Contrary to this, when $R > 200$ for $\sigma = 10$ and $b = 8/3$ [Fig. 6 (top panel)] $\eta_{y^3}^{\text{man}} > 0.40$ becomes clearly greater than $\eta_{z^3}^{\text{man}} \approx 0.20$. We have here a clear dependency of the observability on the underlying dynamics, a feature which seems to be rather marginal. We could also mention the stiff variation observed when the symmetry of the attractor is broken (occurring for $R \in [141; 167]$ and for $R > 203$; bifurcation diagrams not shown) Before starting our interpretation of the class of synchronization in terms of observability coefficients, it should be pointed out that assessing the observability of a system with symmetry properties is not a trivial problem and is still an open problem [23].

When Lorenz systems are coupled by using variable x or y, the MSFs clearly suggest a class I synchronization, independently of the dynamics investigated [Figs. 7(a) and 7(b)]. As already mentioned, μ values at which the MSF stability functions $\Lambda_s(\mu)$ become negative should not be interpreted in terms of easiness for synchronizing coupled systems. This is particularly true with the Lorenz system since the visited domain of the state space has a size which strongly depends on parameter values; consequently, variables can evolve over a range which can be drastically affected when parameter values are varied. The coupling parameter required

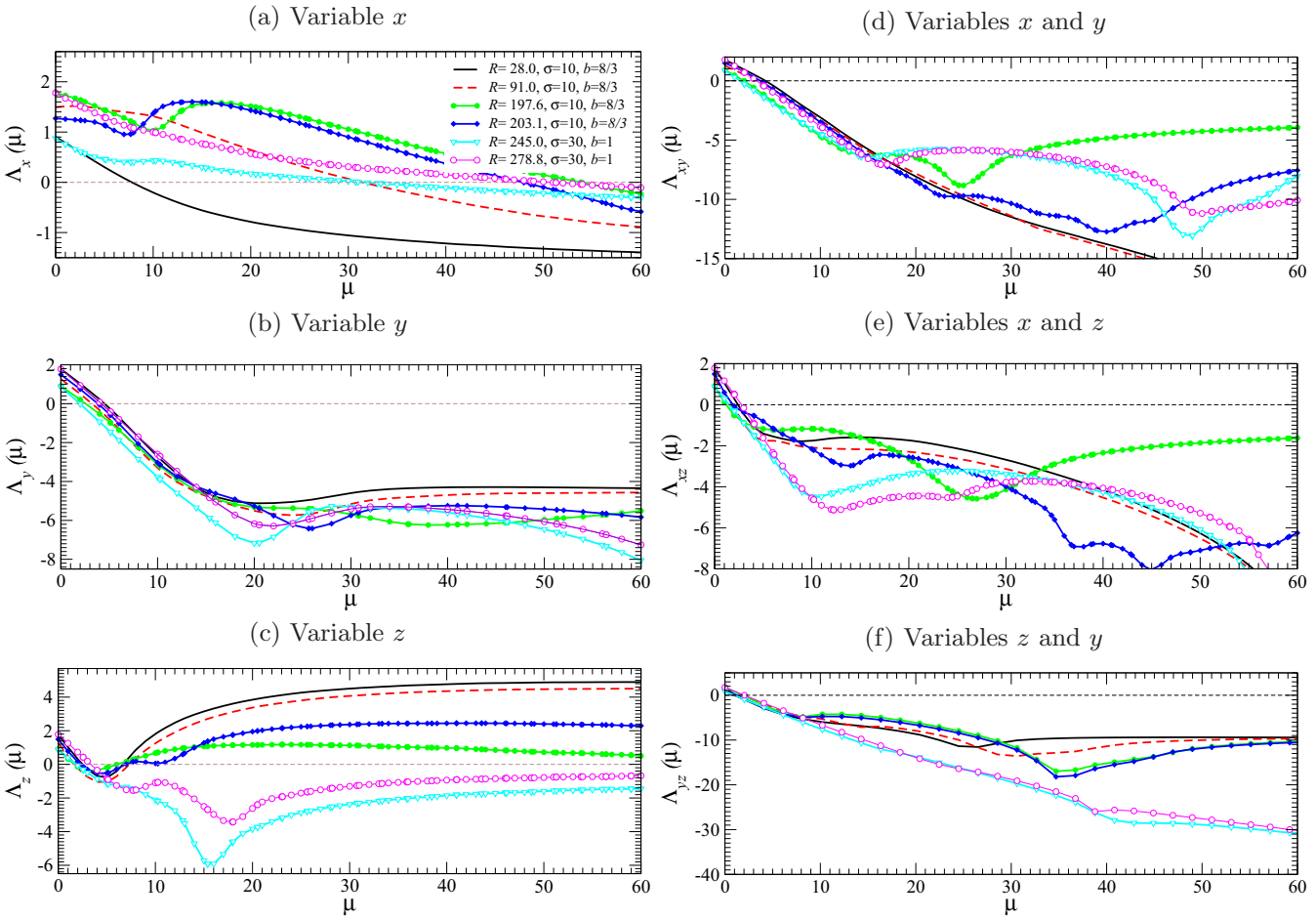

FIG. 7. Master stability functions $\Lambda_s(\mu)$ versus the normalized coupling parameter μ computed for Lorenz systems coupled *via* each of the three variables (a)–(c) and *via* a combination of two of its variables (d)–(f) and for different sets of parameter values [see legend in (a)].

for getting the systems synchronized can be strongly affected by such a dynamical change (to compare different cases, everything should be normalized). What is therefore relevant is the qualitative properties of the MSF, that is, the class to which they belong. In the case of the Lorenz system, the type of MSFs $\Lambda_x(\mu)$ and $\Lambda_y(\mu)$ are not dependent on parameter values and are of class I. This was expected for $\Lambda_x(\mu)$ since variable x provides the best observability of the Lorenz dynamics but this is rather surprising for $\Lambda_y(\mu)$ because the observability provided by variable y is very poor ($\eta_{y^3} = 0.20 < 0.75$).

When variable z is used to couple Lorenz systems, a class II synchronization is obtained [Fig. 7(c)], that is, the synchronization can only be obtained within a limited range $[\mu_m; \mu_M]$. The difficulty for getting a good synchronization with variable z of the Lorenz system is known (even if this was sometimes only implicitly stated) [20,52], and the symmetry property of this system was clearly identified as the cause for this lack of synchronization [53]. The existence of coupling parameter values for which the synchronization can be obtained was nevertheless shown by Huang *et al.* [43] as we checked by computing the distance $\Delta_{12} = \sqrt{(\boldsymbol{x}_1 - \boldsymbol{x}_2)^2}$ between two Lorenz systems (Fig. 8) for which the eigenvalues of the coupling matrix $\boldsymbol{G}$ are $\nu_1 = 0$ and $\nu_2 = 2$. For instance, in the case of the common Lorenz attractor [Fig. 5(a)] there is a quite large range of coupling parameter values leading to a full synchronization [Fig. 8(a)]. Beyond $\epsilon_z = \mu_M/\nu_2 \sim 6.1/2 = 3.1$, the synchronization is rather unstable and, most likely, the results strongly depend on the initial conditions. As mentioned by Balmforth and co-workers [53], this instability results from the fact that variable z is left invariant under the rotation symmetry; in other terms, this means that variable z does not distinguish two symmetry-related states, that is, (x,y,z) from $(-x,-y,z)$. Variable z cannot therefore track properly the transitions from one wing to the other one. The synchronization between Lorenz systems can thus be lost (or retrieved) at each of these transitions (from the z-variable point of view, the difference $|z_1 - z_2|$ is always less than 5% of the range visited; not shown). The saddle point located at the origin of the state space and whose neighborhood is visited when the attractor is bounded by a genus-three torus is directly responsible for these irregular transitions [54].

Consequently, when the saddle point is no longer visited, the transitions occur in a regular way since one revolution in one wing is necessarily followed by a transition in the other wing as observed in the attractors shown in Figs. 5(b) and 5(c). With such attractors, the coupling term is no longer able to switch the trajectory from one wing to the other, and when the two systems are in a "wing opposition," it always remains like that as clearly shown in the case of the attractor observed for $R = 197.6$ [Fig. 5(b)] and for which the error does not

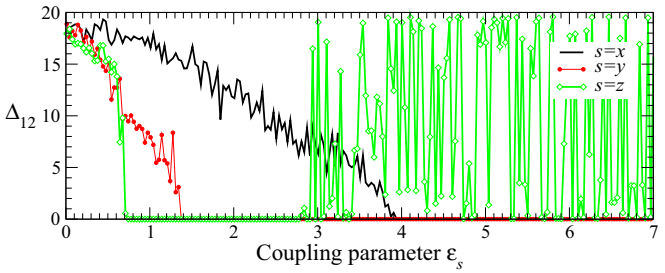

(a) $R = 28$, $\sigma = 10$ and $b = \frac{8}{3}$

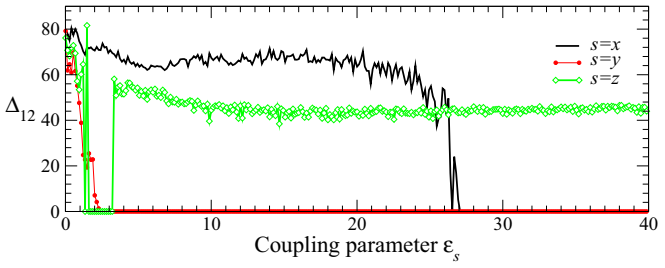

(b) $R = 197.6$, $\sigma = 10$ and $b = \frac{8}{3}$

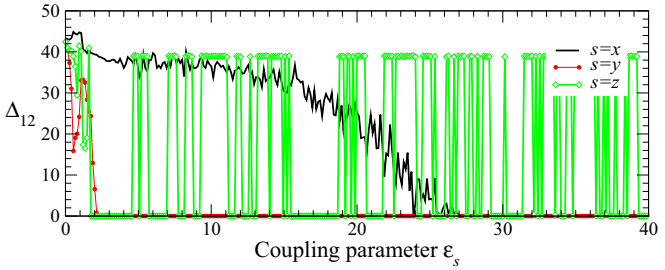

(c) $R = 278.8$, $\sigma = 30$ and $b = 1$

FIG. 8. Distance between two bidirectionally coupled Lorenz systems (slightly detuned) versus the coupling parameter ϵ_s.

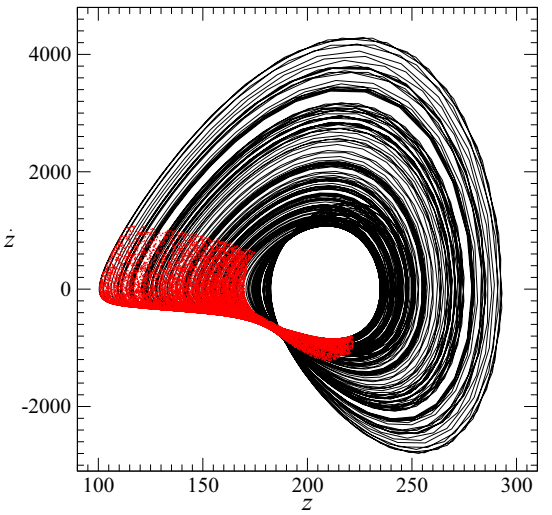

(a) $R = 197.6$, $\sigma = 10$ and $b = \frac{8}{3}$

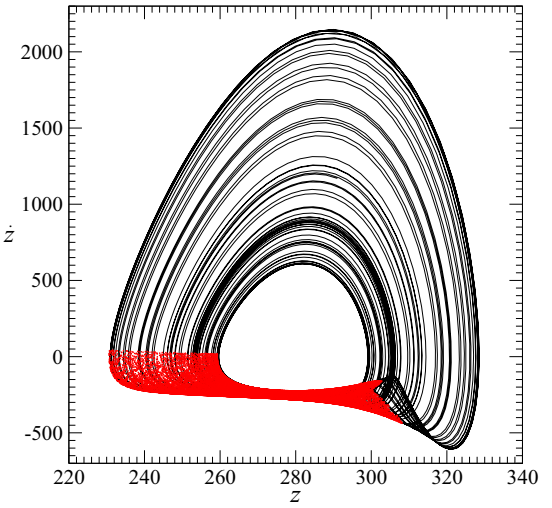

(b) $R = 278.8$, $\sigma = 30$ and $b = 1$

FIG. 9. The chaotic attractors produced by the Lorenz system for two different sets of parameter values. The singular observability manifold $\mathcal{M}_z^{\text{obs}}$ is plotted in red.

depend on the coupling strength when it is greater than a threshold value [green curve in Fig. 8(b)]. For this reason, the class I synchronization obtained for Lorenz systems coupled *via* variable z for $\sigma = 30$ and $b = 1$ [cyan and magenta curves in Fig. 7(c)] as provided by the MSF Λ_z can be explained by the fact that variable z does not detect the difference between the two wings. From a topological point of view, the attractors [Figs. 5(b) and 5(c)] are such as there is necessarily a regular alternation between the left and right wings. Consequently, the type of synchronization for the "Burke and Shaw" attractor [Fig. 5(c)] should not be very different from the type observed for the attractor shown in Fig. 5(b). Nevertheless, it appears that the synchronization is quite easily obtained [for $2 < \epsilon_z < 4$ as shown in Fig. 8(c)] when the Lorenz systems produce the "Burke and Shaw" attractor. For coupling values greater than 4 [Fig. 8(c)], the two Lorenz systems are either synchronized or antiphase synchronized, as confirmed by the error $|z_1 - z_2|$ which vanishes for any $\epsilon_z > 2$ (not shown).

This result could be explained as follows. The dynamics as "seen" by the variable z can be displayed by using the differential embedding $\mathbb{R}^3(z,\dot{z},\ddot{z})$: In such a representation, which provides the so-called *image* of the attractor with no residual symmetry [50], a single "wing" is observed. The image of the two attractors here discussed is shown in Fig. 9. We also reported the points (in red) belonging to the neighborhood of the singular observability manifold $\mathcal{M}_z^{\text{obs}}$. In the case of the attractor shown in Fig. 9(a), the folding occurs outside from the neighborhood of $\mathcal{M}_z^{\text{obs}}$, that is, mostly located at the top of the central hole. By definition, this folding induces the mixing between the trajectories and is associated with a domain rather difficult to control. Contrary to this, in the attractor shown in Fig. 5(b), the folding is located in the neighborhood of the singular observability manifold $\mathcal{M}_z^{\text{obs}}$: The difficult part of the attractor to control is therefore not observable and does not perturb the synchronization. This could also explain why the "Burke and Shaw" attractor [Fig. 5(c)] is associated with a class I synchronization while the Lorenz attractor [Fig. 5(b)] induces a class II synchronization.

The MSF Λ_y suggests that coupling Lorenz systems through the y variable is the best option when a single coupling variable is considered: Adding a second coupling variable does not significantly improve the quality of synchronization [see

Figs. 7(d) and 7(f)]. Contrary to this, when variable x or z is used, it can be a good strategy to add one of the two other variables to improve the negativity of the MSF. This would suggest that when the synchronization is class II or class III, adding a component to the coupling function can help to improve the quality of the synchronization.

C. Coupled Hindmarsh-Rose systems

Finally, we take into consideration the case of networked Hindmarsh-Rose systems. Historically, the Hindmarsh-Rose system originated from the Hodgkin-Huxley model [55], where Richard FitzHugh introduced a second-order differential equation [56], and James Hindmarsh and Malcom Rose added a third equation to limit the neuron firing [57]. The resulting model reads as

$$\begin{aligned} \dot{x} &= I + bx^2 - ax^3 + y - z, \\ \dot{y} &= c - dx^2 - y, \\ \dot{z} &= r[s(x - X_c) - z], \end{aligned} \tag{20}$$

where x is the membrane potential, y the recovery variable (quantifying the transport of sodium and potassium through fast ion channels), and z an adaptation current which gradually hyperpolarizes the cell (it corresponds to the transport of other ions through slow channels). For appropriate parameter values, the Hindmarsh-Rose system produces a chaotic attractor characterized by a first-return map which is smooth and unimodal. This behavior is obtained after a period-doubling cascade when the applied current I is decreased.

The symbolic observability coefficients for the Hindmarsh-Rose system are

$$\eta^{\text{sym}}_{z^3} = 1 > \eta^{\text{sym}}_{y^3} = 0.56 > \eta^{\text{sym}}_{x^3} = 0.25.$$

Nevertheless, there is here the first example where a symbolic observability coefficient does not assess correctly the actual observability since $\eta^{\text{sym}}_{x^3}$ should be equal to 1, Φ_x defining a global diffeormorphism. In the subsequent part of this paper, the corrected value $\eta^{\text{sym}}_{x^3} = 1$ will be used. Indeed, this is a very rare situation where two non-trivial nonlinear terms vanish each other, thus leading to a constant determinant Det $\mathcal{J}_{\phi_x} = r - 1$. The map,

$$\Phi^3_x = \begin{vmatrix} X = x \\ Y = I + bx^2 - ax^3 + y - z \\ Z = (2ax - 3x^3)(y + ax^2 - x^3 - z + I) \\ \quad +1 - d^2x - r(s(x - X_e) - z) \end{vmatrix}, \tag{21}$$

has a Jacobian matrix $\mathcal{J}_{\Phi^3_x} = \mathcal{O}^3_x$ equal to

$$\begin{bmatrix} 1 & 0 & 0 \\ 2ax - 3x^2 & 1 & -1 \\ J_{13} & 2ax - 3x^2 - 1 & -2ax + 3x^2 + r \end{bmatrix}, \tag{22}$$

where J_{13} is too complex and not sufficiently relevant for being here reported, and whose determinant is

$$\begin{aligned} \text{Det}\mathcal{J}_{\Phi^3_x} &= [-2ax + 3x^2 + r + 2ax - 3x^2 - 1] \\ &= r - 1. \end{aligned} \tag{23}$$

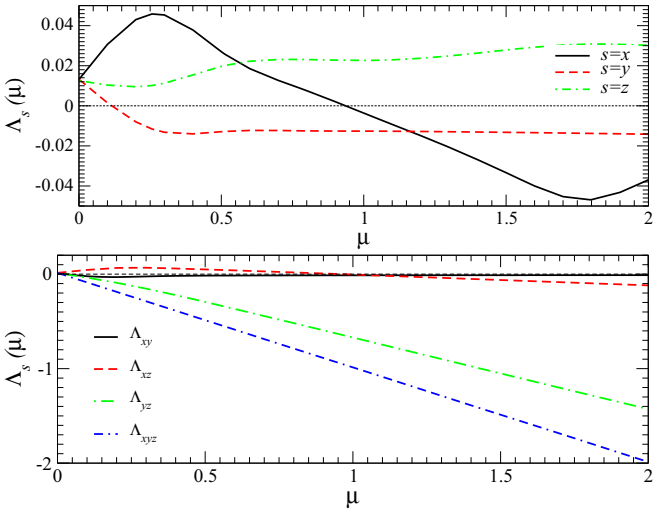

FIG. 10. Master stability functions $\Lambda_s(\mu)$ versus the normalized coupling parameter μ for the Hindmarsh-Rose systems coupled *via* each one of the three variables (top panel) and *via* a combination of two and three of its variables (bottom panel). Parameter values are as follows: $a = 1, b = 3, c = 1, d = 5, r = 0.001, s = 4, X_c = -\frac{1+\sqrt{5}}{2}$, and $I = 3.318$.

The Hindmarsh-Rose system has therefore two variables (x and z) providing a full observability, and one associated with the singular observability manifold,

$$\mathcal{M}^{\text{obs}}_y = \{(x, y, z) \in \mathbb{R}^3 | x = \pm\sqrt{d}\}. \tag{24}$$

According to the corrected symbolic coefficient, variables x and z should provide a class I synchronizability.

The MSF $\Lambda_s(\mu)$ (top panel of Fig. 10) indicates that variables x and y lead to a class I synchronization. Nevertheless, and contrary to our expectations, when coupled *via* variable z, Hindmarsh-Rose systems cannot be synchronized. This is confirmed by computing the distance Δ_{12} between two slightly detuned Hindmarsh-Rose systems (Fig. 11) which never vanishes although the error $|z_1 - z_2|$ (not shown) converges to zero.

In this latter case, the difficulty encountered comes from the fact that the dynamics underlying variable z is very slow compared to those underlying the two other variables (Fig. 12): There is therefore a delay in the action, particularly when the very stiff evolution of variables x and y occur. The origin of the

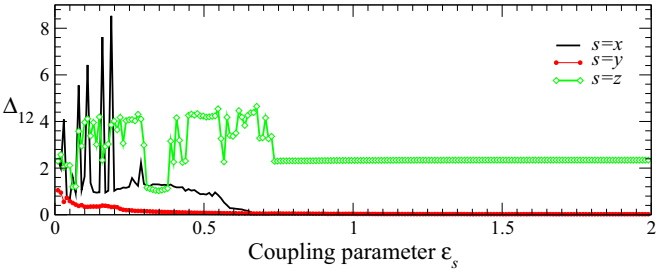

FIG. 11. Distance between two bidirectionally coupled Hindmarsh-Rose systems (slightly detuned) versus the coupling parameter ρ_s. Same parameter values as in Fig. 10.

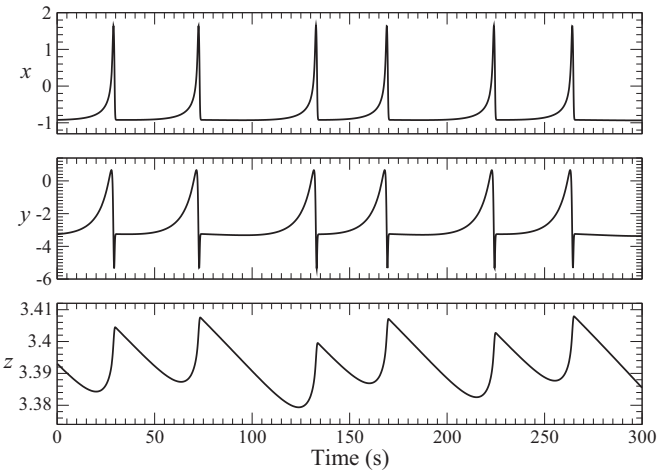

FIG. 12. Time series for the three variables of the Hindmarsh-Rose system. Same parameter values as in Fig. 10.

lack of synchronization is here again dynamical (as observed when Lorenz systems were coupled by variable z) and not structural as observed when Rössler systems were coupled *via* variable z.

From the class of synchronization point of view, coupling Hindmarsh-Rose systems *via* variable x or y is already an optimal solution since both types of coupling lead to a class I synchronization. Adding a second coupling variable to variable x does not significantly improve the negativity of the MSF. The observability coefficient $\eta^{\mathrm{sym}}_{x^3} = 1$ could explain this feature. The symbolic coefficient $\eta^{\mathrm{sym}}_{y^3} = 0.56$, that is, not very large, could thus explain also that adding a variable may improve the negativity of the corresponding MSF. Adding variable x is rather useless since it evolves in a rather similar manner as variable y (Fig. 12): The lack of observability is thus not improved. Contrary to this, when the slow variable is added to the fast variable x, this improves clearly the stability of the synchronization (Fig. 10, bottom panel). Adding variable x or y to variable z for coupling Hindmarsh-Rose systems allows one to switch from class III to class I synchronization.

IV. CONCLUSIONS

In this paper we investigated if and how the classes of synchronization, based on the qualitative properties of the MSFs, could be related to the observability coefficients. Several conclusions can be drawn, indicating that a nontrivial relationship exists between observability and class of synchronizability, which certainly will deserve further studies. First, we checked that observability is most often very weakly dependent on parameter values. Consequently, observability coefficients which are not dependent on them are therefore reliable in most of the cases. Second, if the interplay between observability coefficients and the class of synchronization is obvious in the case of simple systems like the Rössler system, the case is much more complicated when Lorenz systems are considered for few different reasons: (i) The rotation symmetry has a strong influence on the synchronizability but is not well taken into account by observability coefficients; (ii) counterintuitively, topological properties of the attractors (as described by template) have not always an effect on the synchronizability. In the case of variable z, a dependence of the class of synchronization on parameter values was observed: It was possible to relate it to the relative location between the observability singular manifold and the folding mechanism of the attractor. This seems to be a rather rare case. In another very particular case, we found that the lack of relation between the observability coefficients and the class of synchronization was induced by very specific and different dynamical properties (different time scales observed for the dynamics underlying each variable of the Hindmarsh-Rose system). To sum up, (i) the observability coefficients explain only partly the class of synchronization, and the remaining part could be related to specific properties of the dynamics under study; (ii) adding more coupling variables does not necessarily improve the quality of synchronization and, actually, it can sometimes degrade it; (iii) the generic way one can choose *a priori* the "best" variables for synchronizing systems deserves further exploration and future work in this direction is underway. In particular, we are investigating whether or not the observability accounts for how the phase is "measured" in a given variable.

ACKNOWLEDGMENTS

Work partly supported by the Spanish Ministry of Economy under Project No. FIS2013-41057-P and by GARECOM, Group of Research Excellence URJC-Banco de Santander.

[1] C. Huygens, *Horologium Oscillatorium* (Parisiis, Paris, 1673); English translation by R. J. Blackwell (Iowa State University Press, Ames, 1986).

[2] I. I. Blekhman, *Selected Topics in Vibrational Mechanics* (World Scientific, Singapore, 2004).

[3] M. Toiya, H. O. González-Ochoa, V. K. Vanag, S. Fraden, and I. R. Epstein, Synchronization of chemical micro-oscillators, J. Phys. Chem. Lett. **1**, 1241 (2010).

[4] E. Rodriguez, N. George, J. P. Lachaux, J. Martinerie, B. Renault, and F. J. Varela, Perception's shadow: long-distance synchronization of human brain activity, Nature (London) **397**, 430 (1999).

[5] An. A. Fingelkurts, Al. A. Fingelkurts, and S. Kähkönen, Functional connectivity in the brain—is it an elusive concept? Neurosc. Biobehav. Rev. **28**, 827 (2005).

[6] I. Sendiña-Nadal, Y. Ofran, J. A. Almendral, J. M. Buldú, I. Leyva, D. Li, S. Havlin, and S. Boccaletti, Unveiling protein functions through the dynamics of the interaction network, PLoS ONE **6**, e17679 (2011).

[7] R. A. Ims and H. P. Andreassen, Spatial synchronization of vole population dynamics by predatory birds, Nature (London) **408**, 194 (2000).

[8] L. Nummenmaa, E. Glerean, M. Viinikainen, I. P. Jääskeläinen, R. Hari, and M. Sams, Emotions promote social interaction

by synchronizing brain activity across individuals, Proc. Natl. Acad. Sci. USA **109**, 9599 (2012).

[9] S. Boccaletti, J. Kurths, G. Osipov, D. L. Valladares, and C. S. Zhou, The synchronization of chaotic systems, Phys. Rep. **366**, 1 (2002).

[10] A. Pikovsky, M. Rosenblum, and J. Kurths, *Synchronisation—A Universal Concept in Nonlinear Sciences* (Cambridge University Press, Cambridge, 2003).

[11] S. Strogatz, *SYNC: The Emerging Science of Spontaneous Order* (Penguin Press Science, London, 2004).

[12] H. Voss, U. Henning, J. Timmer, and J. Kurths, Nonlinear dynamical system identification from uncertain and indirect measurements, Int. J. Bifurcation Chaos **14**, 1905 (2004).

[13] R. Brown, N. F. Rulkov, and E. R. Tracy, Modeling and synchronizing chaotic systems from time series data, Phys. Rev. E **49**, 3784 (1994).

[14] L. A. Aguirre and C. Letellier, Modeling nonlinear dynamics and chaos: A review, Mathe. Prob. Engin. **2009**, 238960 (2009).

[15] T. Stankovski, A. Duggento, P. V. E. McClintock, and A. Stefanovska, Inference of Time-Evolving Coupled Dynamical Systems in the Presence of Noise, Phys. Rev. Lett. **109**, 024101 (2012).

[16] T. Stankovski, P. V. E. McClintock, and A. Stefanovska, Dynamical inference: Where phase synchronization and generalized synchronization meet, Phys. Rev. E **89**, 062909 (2014).

[17] E. Bianco-Martinez, N. Rubido, Ch. G. Antonopoulos, and M. S. Baptista, Successful network inference from time-series data using mutual information rate, Chaos **26**, 043102 (2016).

[18] L. M. Pecora and T. L. Carroll, Master Stability Functions for Synchronized Coupled Systems, Phys. Rev. Lett. **80**, 2109 (1998).

[19] S. Boccaletti, V. Latora, Y. Moreno, M. Chavez, and D.-U. Hwang, Complex networks: Structure and dynamics, Phys. Rep. **424**, 175 (2006).

[20] L. M. Pecora and T. L. Carroll, Synchronization in Chaotic Systems, Phys. Rev. Lett. **64**, 821 (1990).

[21] G. V. Osipov, A. S. Pikovsky, M. G. Rosenblum, and J. Kurths, Phase synchronization effects in a lattice of nonidentical Rössler oscillators, Phys. Rev. E **55**, 2353 (1997).

[22] R. Hermann and A. Krener, Nonlinear controllability and observability, IEEE Trans. Auto. Control **22**, 728 (1977).

[23] C. Letellier and L. A. Aguirre, Investigating nonlinear dynamics from time series: the influence of symmetries and the choice of observables, Chaos **12**, 549 (2002).

[24] C. Letellier, L. A. Aguirre, and J. Maquet, Relation between observability and differential embeddings for nonlinear dynamics, Phys. Rev. E **71**, 066213 (2005).

[25] Y.-Y. Liu, J.-J. Slotine, and A.-L. Barabási, Observability of complex systems, Proc. Natl. Acad. Sci. USA **110**, 2460 (2012).

[26] A. J. Whalen, S. N. Brennan, T. D. Sauer, and S. J. Schiff, Observability and Controllability of Nonlinear Networks: The Role of Symmetry, Phys. Rev. X **5**, 011005 (2015).

[27] A. Chamseddine, H. Noura, M. Ouladsine, and T. Raharijaona, Observability of complex systems: Minimal cost sensor network design, IFAC Proceedings **41**, 13287 (2008).

[28] G. Yan, G. Tsekenis, B. Barzel, J.-J. Slotine, Y.-Y. Liu, and A.-L. Barabási, Spectrum of controlling and observing complex networks, Nat. Phys. **11**, 779 (2015).

[29] P. J. Menck, J. Heitzig, J. Kurths, and H. J. Schellnhuber, How dead ends undermine power grid stability, Nat. Commu. **5**, 3969 (2014).

[30] C. Letellier, L. A. Aguirre, and J. Maquet, How the choice of the observable may influence the analysis of nonlinear dynamical systems, Commun. Nonlinear Sci. Numer. Simul. **11**, 555 (2006).

[31] H. Yang, F. Zhao, and B. Wang, Synchronizabilities of networks: A new index, Chaos **16**, 043112 (2006).

[32] L. Abbas, J. Demongeot, and N. Glade, Synchrony in reaction-diffusion models of morphogenesis: applications to curvature-dependent proliferation and zero-diffusion front waves, Philos. Trans. R. Soc. London A **367**, 4829 (2009).

[33] A. Zeng, Y. Hu, and Z. Di, Optimal tree for both synchronizability and converging time, Europhys. Lett. **87**, 48002 (2009).

[34] G. Zhang, Z. Ma, Y. Wang, and J. Zhang, Partial synchronizability characterized by principal quasi-submatrices corresponding to clusters, Abstr. Appl. Anal. **2014**, 584790 (2014).

[35] C. Letellier and L. A. Aguirre, On the interplay among synchronization, observability and dynamics, Phys. Rev. E **82**, 016204 (2010).

[36] L. A. Aguirre and Letellier, Controllability and synchronizability: Are they related? Chaos Solitons Fractals **83**, 242 (2016).

[37] F. Takens, Detecting strange attractors in turbulence, Lect. Notes Math. **898**, 366 (1981).

[38] C. T. Chen, *Linear Systems Theory and Design*, 3rd ed. (Oxford University Press, London, 1999).

[39] The Lie derivative of the ith component of the vector field $\boldsymbol{f}$ is defined as

$$\mathcal{L}_{f_i}(\boldsymbol{x}) = \sum_{k=1}^{m} f_k \frac{\partial f_i(\boldsymbol{x})}{\partial x_k}.$$

Higher-order derivatives are given recursively according to

$$\mathcal{L}^n_{f_i}(\boldsymbol{x}) = \mathcal{L}_{f_i}\left[\mathcal{L}^{n-1}_{f_i}(\boldsymbol{x})\right].$$

[40] E. Bianco-Martinez, M. S. Baptista, and C. Letellier, Symbolic computations of non-linear observability, Phys. Rev. E **91**, 062912 (2015).

[41] C. Letellier and L. A. Aguirre, Symbolic observability coefficients for univariate and multivariate analysis, Phys. Rev. E **79**, 066210 (2009).

[42] M. Frunzete, J.-P. Barbot, and C. Letellier, Influence of the singular manifold of nonobservable states in reconstructing chaotic attractors, Phys. Rev. E **86**, 026205 (2012).

[43] L. Huang, Q. Chen, Y.-C. Lai, and L. M. Pecora, Generic behavior of master-stability functions in coupled nonlinear dynamical systems, Phys. Rev. E **80**, 036204 (2009).

[44] O. E. Rössler, An equation for continuous chaos, Phys. Lett. A **57**, 397 (1976).

[45] C. Letellier, P. Dutertre, and B. Maheu, Unstable periodic orbits and templates of the Rössler system: toward a systematic topological characterization, Chaos **5**, 271 (1995).

[46] J. D. Farmer, J. P. Crutchfield, H. Frœling, N. H. Packard, and R. S. Shaw, Power spectra and mixing properties of strange attractors, Ann. N.Y. Acad. Sci. **357**, 453 (1980).

[47] R. Sevilla-Escoboza, R. Gutiérrez, G. Huerta-Cuellar, S. Boccaletti, J. Gómez-Gardeñes, A. Arenas, and J. M. Buldú,

Enhancing the stability of the synchronization of multivariable coupled oscillators, Phys. Rev. E **92**, 032804 (2015).
[48] E. N. Lorenz, Deterministic nonperiodic flow, J. Atmos. Sci. **20**, 130 (1963).
[49] C. Letellier, P. Dutertre, and G. Gouesbet, Characterization of the Lorenz system taking into account the equivariance of the vector field, Phys. Rev. E **49**, 3492 (1994).
[50] C. Letellier and R. Gilmore, Covering dynamical systems: Two-fold covers, Phys. Rev. E **63**, 016206 (2001).
[51] C. Letellier, P. Dutertre, J. Reizner, and G. Gouesbet, Evolution of multimodal map induced by an equivariant vector field, J. Phys. A **29**, 5359 (1996).
[52] J. Alvarez, Synchronization in the Lorenz system: Stability and robustness, Nonlinear Dynamics **10**, 89 (1996).
[53] N. Balmforth, C. Tresser, P. Worfolk, and C. Wah Wu, Master-slave synchronization and the Lorenz equations, Chaos **7**, 392 (1997).
[54] C. Letellier, T. Tsankov, G. Byrne, and R. Gilmore, Large-scale structural reorganization of strange attractors, Phys. Rev. E **72**, 026212 (2005).
[55] A. L. Hodgkin and A. F. Huxley, A quantitative description of membrane current and its application to conduction and excitation in nerve, J. Physiol. **117**, 500 (1952).
[56] R. FitzHugh, Impulses and physiological states in theoretical models of nerve membrane, Biophys. J. **1**, 445 (1961).
[57] J. L. Hindmarsh and R. M. Rose, A model of neuronal bursting using three coupled first order differential equations, Proc. R. Soc. London B **221**, 87 (1984).